Mon. Not. R. Astron. Soc. **348,** L43–L48 (2004) doi:10.1111/j.1365-2966.2004.07567.x

Radiative transfer through the intergalactic medium

James Bolton,[1] Avery Meiksin[2]★ and Martin White[3]

[1] *Institute of Astronomy, University of Cambridge, The Observatories, Madingley Road, Cambridge CB3 0HA*
[2] *Institute for Astronomy, University of Edinburgh, Blackford Hill, Edinburgh EH9 3HJ*
[3] *Departments of Astronomy and Physics, University of California, Berkeley, CA 94720, USA*

Accepted 2003 December 18. Received 2003 December 8; in original form 2003 October 22

ABSTRACT

We use a probabilistic method to compute the propagation of an ionization front corresponding to the reionization of the intergalactic medium in a Λ-cold dark matter (ΛCDM) cosmology, including both hydrogen and helium. The effects of radiative transfer substantially boost the temperature of the ionized gas over the case of uniform reionization. The resulting temperature–density relation of the ionized gas is both non-monotonic and multiple-valued, reflecting the non-local character of radiative transfer and suggesting that a single polytropic relation between local gas density and temperature is a poor description of the thermodynamical state of baryons in the post-reionization universe.

Key words: methods: numerical – intergalactic medium – quasars: absorption lines.

1 INTRODUCTION

Hydrodynamical simulations of structure formation in the Universe have led to fundamental insights into the structure and evolution of the intergalactic medium (IGM) (Cen et al. 1994; Zhang, Anninos & Norman 1995; Hernquist et al. 1996; Bond & Wadsley 1997; Zhang et al. 1997; Theuns, Leonard & Efstathiou 1998). Comparisons with the Lyα forest, as measured in high redshift quasi-stellar object (QSO) spectra, show that the simulations broadly reproduce the statistical properties of the IGM. Precision comparisons with the highest spectral resolution measurements recover the cumulative flux distributions and H I column density distributions to an accuracy of a few per cent (Meiksin, Bryan & Machacek 2001). More problematic are the predicted widths of the absorption features, which appear to require additional sources of broadening, perhaps late He II reionization, to match the measured widths (Theuns et al. 1999; Bryan & Machacek 2000; Meiksin et al. 2001).

Many of the properties of the IGM may be attributed to the gravitational instability of the dark matter alone, as the baryon density fluctuations closely follow those of the dark matter (Zhang et al. 1998). This has led to the development of pseudo-hydrodynamic simulations based on pure gravity, in which the baryon fluctuations are assumed to follow the dark matter exactly and the temperature is assumed to be derived from an effective equation of state (Petitjean, Mücket & Kates 1995; Croft et al. 1998; Gnedin & Hui 1998; Meiksin & White 2001). In recent years, such simulations have been increasingly relied on for predicting the flux power spectrum of the Lyα forest (Meiksin & White 2001; Zaldarriaga, Hui & Tegmark 2001; Croft et al. 2002; Meiksin & White 2004; Seljak, McDonald & Makarov 2003).

★E-mail: aam@roe.ac.uk

The simulations have generally been done assuming sudden early homogeneous H I and He II reionization. Although tentative steps have been taken to introduce radiative transfer into the simulations using approximate schemes (Abel, Norman & Madau 1999; Gnedin & Abel 2001; Nakamoto, Umemura & Susa 2001; Ciardi, Stoehr & White 2003), these simulations have emphasized the propagation of H I ionization fronts and the predicted mean optical depths. Except for the simulations of Gnedin & Abel, they have not solved fully self-consistently for the combined gas dynamics and radiative transfer.

In this Letter, we extend the photon-conserving scheme of Abel et al. to include the treatment of helium and explore the thermal effects of radiative transfer in the inhomogeneous medium predicted in a Λ-cold dark matter (ΛCDM) cosmology.

2 RADIATIVE TRANSFER

2.1 Simulation data

We use the data from a previously run ΛCDM simulation used to investigate effects of radiative transfer on the Lyα forest (Meiksin & White 2004). The simulation was run using a pure particle mesh (PM) dark matter code, and it was assumed that the gas and the dark matter have the same spatial distribution. A description of the parallel PM code is given in Meiksin & White (2003). The parameters used for the simulation are $\Omega_{\rm m} = 0.30, \Omega_\Lambda = 0.70$, $\Omega_{\rm b} = 0.045$, $h = H_0/100\ {\rm km\ s^{-1}\ Mpc^{-1}} = 0.70$, and slope of the primordial density perturbation power spectrum $n = 1.05$. The model is consistent with existing large-scale structure, Lyα forest flux distribution, cluster abundance and *Wilkinson Microwave Anisotropy Probe* (*WMAP*) constraints (Meiksin & White 2004). The simulation was run using 512^3 particles and a 1024^3 force mesh, in a cubic box with (comoving) side length 25 h^{-1} Mpc, adequate for obtaining converged estimates of the Lyα pixel flux distribution and flux power spectrum

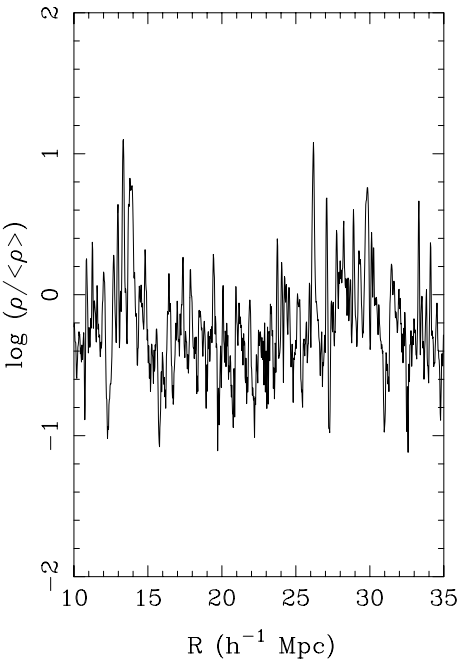

Figure 1. The baryon density fluctuations at $z = 6$ against comoving distance from the ionizing source for the line of sight considered in our radiative transfer simulations.

(Meiksin & White 2003, 2004). A typical line-of-sight density run at $z = 6$, used for the radiative transfer calculations here, is shown in Fig. 1.

2.2 Equations of radiative transfer

To consider the effect of radiative transfer when modelling the propagation of ionization fronts (I-fronts) into the IGM, we extend the photon-conserving algorithm of Abel et al. to include helium. The advantage of this scheme is that energy is conserved independently of numerical resolution, ensuring that I-fronts propagate at the correct speeds in our simulations. In practice, this means that larger step sizes may be taken on the simulation space grid without the associated loss of accuracy which would occur when solving the radiative transfer equation through direct numerical integration.

The probabilities for the absorption of an ionizing photon by H I, He I and He II, respectively, are

$$P_{\rm abs}^{\rm H\,I} = p_{\rm H\,I} q_{\rm He\,I} q_{\rm He\,II} \left[1 - \exp\left(-\tau_\nu^{\rm tot}\right)\right]/D, \tag{1}$$

$$P_{\rm abs}^{\rm He\,I} = q_{\rm H\,I} p_{\rm He\,I} q_{\rm He\,II} \left[1 - \exp\left(-\tau_\nu^{\rm tot}\right)\right]/D, \tag{2}$$

$$P_{\rm abs}^{\rm He\,II} = q_{\rm H\,I} q_{\rm He\,I} p_{\rm He\,II} \left[1 - \exp\left(-\tau_\nu^{\rm tot}\right)\right]/D. \tag{3}$$

Here we have defined the auxiliary absorption and transmission probabilities $p_i = 1 - \exp(-\tau_\nu^i)$, $q_i = \exp(-\tau_\nu^i)$, with i denoting the species being referred to, $\tau_\nu^{\rm tot} = \tau_\nu^{\rm H\,I} + \tau_\nu^{\rm He\,I} + \tau_\nu^{\rm He\,II}$, where τ_ν^i is the optical depth for a given species, and $D = p_{\rm H\,I} q_{\rm He\,I} q_{\rm He\,II} + q_{\rm H\,I} p_{\rm He\,I} q_{\rm He\,II} + q_{\rm H\,I} q_{\rm He\,I} p_{\rm He\,II}$. These probabilities can be used to calculate the ionization rate for a given species per unit volume, $n_i \Gamma_i$, as follows. If in a time δt, $\delta t \dot{N}_\nu^{l-1}$ photons enter grid zone l from zone $l - 1$, then the number of photons that will be absorbed in zone l by species i is $\delta t \dot{N}_\nu^{l-1} P_{\rm abs}^i$, where $P_{\rm abs}^i$ is the absorption probability for species i within zone l. The ionization rate of species i in zone l of volume V^l is then

$$n_i^l \Gamma_i^l = \frac{1}{V^l} \sum_g \dot{N}_{\nu_g}^{l-1} P_{\rm abs}^i(\nu_g), \tag{4}$$

where we have divided the frequencies into 100 discrete groups g evenly spaced between $\nu_L^{\rm H\,I}$ and $10\nu_L^{\rm H\,I}$. (Although we found this spacing to be adequate, we have made no attempt to optimize it.) These are used in the following set of coupled equations to solve for the positions of the three I-fronts over time:

$$\frac{{\rm d}n_{\rm H\,II}}{{\rm d}t} = n_{\rm H\,I}\Gamma_{\rm H\,I} - n_e n_{\rm H\,II}\alpha_{\rm H\,I}(T) - 3\frac{\dot{a}}{a} n_{\rm H\,II}, \tag{5}$$

$$\frac{{\rm d}n_{\rm He\,II}}{{\rm d}t} = n_{\rm He\,I}\Gamma_{\rm He\,I} + n_e n_{\rm He\,III}\alpha_{\rm He\,II}(T) - n_{\rm He\,II}\Gamma_{\rm He\,II} - n_e n_{\rm He\,II}\alpha_{\rm He\,I}(T) - 3\frac{\dot{a}}{a} n_{\rm He\,II}, \tag{6}$$

$$\frac{{\rm d}n_{\rm He\,III}}{{\rm d}t} = n_{\rm He\,II}\Gamma_{\rm He\,II} - n_e n_{\rm He\,III}\alpha_{\rm He\,II}(T) - 3\frac{\dot{a}}{a} n_{\rm He\,III}, \tag{7}$$

where n_i denotes number density, Γ_i (s^{-1}) is the photoionization rate per atom, $\alpha_i(T)$ is the total radiative recombination coefficient and a is the cosmological expansion factor.

The time evolution of the gas temperature T is given by

$$\frac{{\rm d}T}{{\rm d}t} = \frac{2(G - L)}{3kn} + \frac{T}{n}\frac{{\rm d}n_e}{{\rm d}t} - 3\frac{\dot{a}}{a}\left(\frac{2}{3}T + \frac{n_e}{n}T\right). \tag{8}$$

where $n = n_{\rm H\,I} + n_{\rm He\,I} + n_{\rm H\,II} + n_{\rm He\,II} + n_{\rm He\,III} + n_e$, $n_e = n_{\rm H\,II} + n_{\rm He\,II} + 2n_{\rm He\,III}$, k is the Boltzmann constant, and G and L (J m^{-3} s^{-1}) are the atomic heating and cooling rates, respectively. The last term is the adiabatic cooling term resulting from cosmological expansion, which will dominate the thermal effects of gas motions at the densities we consider. While computing the photoionization, we assume the gas overdensity (not the density) stays frozen, which is a good approximation on the scales relevant to the Lyα forest (Zhang et al. 1998). As in similar previous studies, we do not include the effects of adiabatic compression heating, as this will only affect the temperature for the relatively rare virialized haloes with circular velocities exceeding $\sim$20 km s^{-1} (Meiksin 1994; Meiksin & White 2004).

The heating rate G^l in cell l is due to the photoionization of H I, He I and He II according to $G^l = G^l_{\rm H\,I} + G^l_{\rm He\,I} + G^l_{\rm He\,II}$, where for each species i, G_i^l is evaluated in a similar manner to the ionization rate per unit volume as given in equation (4),

$$n_i^l G_i^l = \frac{1}{V^l} \sum_g (h\nu_g - \chi_i) \dot{N}_{\nu_g}^{l-1} P_{\rm abs}^i(\nu_g), \tag{9}$$

where χ_i is the ionization potential of species i. The atomic cooling rate L includes radiative recombination cooling to H I, He I and He II, electron excitation of H I, and Compton cooling off the cosmic microwave background photons. The radiative recombination and cooling rates are taken from Meiksin (1994).

Equations (5)–(8) are solved using explicit forward Euler integration. Although an implicit numerical scheme such as backward Euler integration results in a more stable solution at low numerical resolution (Anninos et al. 1997), we find that to obtain the required numerical accuracy as well as to maintain stability, both methods require similar numerical resolution. For the sake of speed and simplicity, the forward method is preferred. The time-step is restricted to being no more than several times greater that the hydrogen ionization time-scale, $\Gamma_{\rm H\,I}^{-1}$, for numerical accuracy.

We take the frequency-specific luminosity of the ionizing source in our simulations to be described by a power-law spectrum with

index $\alpha = 1.5$, and a luminosity of $L_\nu^{\rm Q} = 10^{23}$ W Hz^{-1} at the Lyman edge. This spectrum is typical of that of QSOs, which are probable candidate sources for contributing to the reionization of the IGM. The assumed mass fraction of helium in the IGM is $Y \simeq 0.235$.

We tested the photon-conserving algorithm on the photoionization of gas with uniform density around a point source. The resulting solutions for the ionization and temperature profiles were accurate to better than 10 per cent for optical depths at the Lyman edge of up to $\Delta\tau_\nu \simeq 20$ per cell on the space grid. This results in a significant reduction in the computational demands compared with a radiative transfer scheme in which the ionization rates are computed by direct numerical integration over the intensity $[L_\nu^{\rm Q} e^{-\tau_\nu}/(4\pi r)^2]$ and photoionization cross-sections (e.g. Madau, Meiksin & Rees 1997). Typically, we find that to obtain an accuracy comparable to the photon-conserving scheme at $\Delta\tau_\nu^{\rm H\,I} \simeq 20$, a direct integration algorithm requires $\Delta\tau_\nu^{\rm H\,I} \simeq 1/4$ in each cell. For the simulation results presented in this Letter, the original PM grid of 1024 separate cells was used over a line of sight 25 h^{-1} comoving Mpc in length. This provided accurate spatial resolution, as at most $\Delta\tau_\nu^{\rm H\,I} \simeq 6.8$ in each cell at the average baryonic density assumed for the neutral IGM at $z = 6$.

3 RESULTS

We set up a problem of a QSO source of luminosity $L_\nu^{\rm Q}$ at $z = 6$ placed at a comoving distance of 10 h^{-1} Mpc from the left edge of the density run shown in Fig. 1, and assume the gas surrounding the QSO up to that point has already been ionized. Placing the source at this distance avoids having to impose the restriction that the I-fronts propagate no faster than the speed of light. We indicate the displaced position of the source in the figures by starting the (comoving) spatial axes at $R = 10\ h^{-1}$ Mpc.

Two cases were compared: computing the ionization and temperature profiles by incorporating radiative transfer as discussed in Section 2.2 (hereafter the RT simulation); and a second case neglecting radiative transfer, assuming instead an instantaneous uniform ionization rate across the whole line of sight (hereafter the nRT simulation), as is usually done in simulations of the Lyα forest. Our intention is to compare the final gas temperatures to determine how large an effect including radiative transfer may have.

Fig. 2 shows a comparison between the IGM temperatures at $z = 5$ computed with and without radiative transfer. The inclusion of radiative transfer results in a significant boost to the temperature of the ionized IGM, a point illustrated by Abel & Haehnelt (1999) in the context of a smooth IGM. The positions of the H II and He II I-fronts at $z = 5$ in the RT simulation are 24 h^{-1} comoving Mpc from the source, while the He III front lags behind at about 19 h^{-1} comoving Mpc; their speeds of propagation are limited by the reduction in the ionization rate caused by the increasing optical depth through the box. Consequently, the heating of the IGM, which we find to be dominated by the photoionization of neutral hydrogen at the H II I-front, is also constrained to lie behind the H II I-front. All gas beyond 24 h^{-1} Mpc is still much cooler. In contrast, the temperature computed by the nRT simulation is much lower and the heating extends across the whole line of sight. The temperature is also much less sensitive to variations in the gas density for the nRT simulation. Fig. 3 compares the results obtained at $z = 3$. By this time, both the H II and He II I-fronts have reached 35 h^{-1} Mpc from the source. The material which has been ionized early on in the RT simulation is now beginning to cool to the same temperature as that computed by the nRT simulation, although the temperature differences remain large. In particular, the gas that was photoionized at $z = 5$ ($R < 24\ h^{-1}$ Mpc), remains nearly twice as hot as the uniformly ionized gas by $z = 3$. In contrast, the regions which were ionized more recently are much hotter than for the nRT simulation. We find that only by $z = 1$, once the gas has been in an ionized state for a sufficiently long period of time, do the temperatures predicted in the two scenarios converge.

The reason for the temperature boost in the RT simulation is made clear by considering the energy per ionization ($E = G/\Gamma$) at

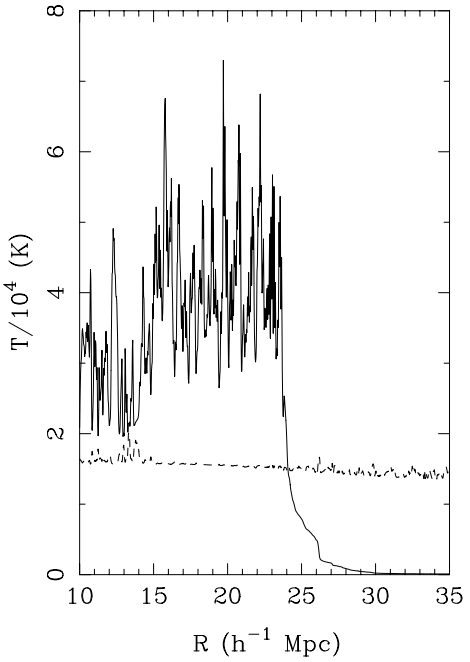

Figure 2. Comparison of the IGM temperature at $z = 5$ against comoving distance from the ionizing source. The solid line is computed using radiative transfer, whereas the dashed-line result assumes a uniform ionization field through the entire line of sight.

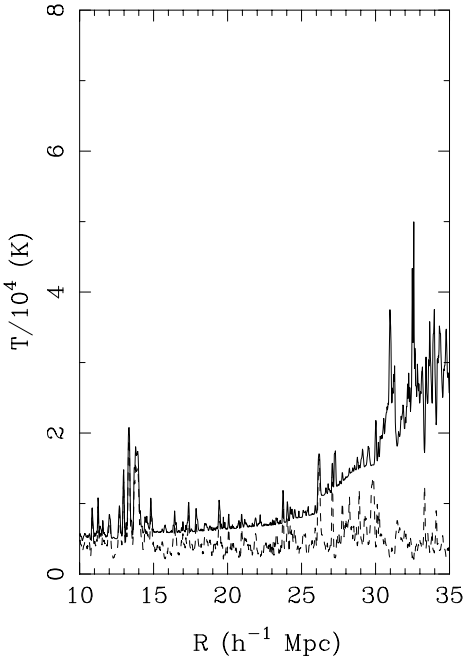

Figure 3. Comparison of the IGM temperature at $z = 3$ against comoving distance from the ionizing source. The line types are as in Fig. 2.

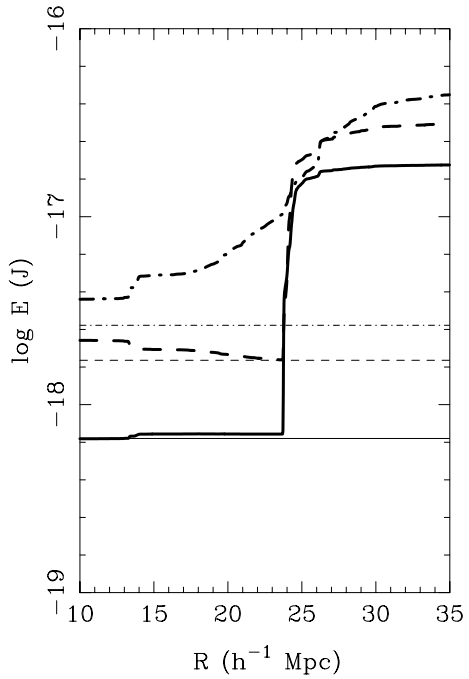

Figure 4. Plot of the energy per ionization for H I (solid line) He I (dashed line) and He II (dot–dashed line) at $z = 5$. The bold lines correspond to the results computed using radiative transfer, whereas the lighter (flat) lines correspond to the uniform ionization field.

the I-front. In Fig. 4, we show that the average energy of a photon absorbed by either H I, He I or He II increases at the relevant I-front, as proportionally more of the lower energy photons have been absorbed already – a consequence of including radiative transfer. This increase to the heating energy per ionization is responsible for the temperature boost. The assumption of an instantaneous ionization field across the line of sight results in an underestimate of the IGM temperature at high redshift.

A comparison of the IGM temperature–density relation computed by the two different simulations is made in Figs 5–7. Only data points where He II has been 90 per cent ionized are plotted, so that gas which is neutral or in the process of being ionized is not considered. In Fig. 5, the underdense regions in the line of sight (Fig. 1) are initially heated to a higher temperature in the RT simulation. A non-monotonic temperature–density relation results. The relation actually splits into two trends. To understand the origin of the split, we divide the data points into two distinct sets corresponding to two regions in which the average density fluctuations are slightly higher or lower than the overall average in the line of sight (see the caption to Fig. 5). The gas in the more dense region, which is closer to the source and thus is ionized sooner, shows the same overall trend as the gas in the less dense region but is slightly cooler at a fixed overdensity. In contrast, in the nRT simulation, the temperature–density relation is both monotonic and essentially single-valued. By $z = 3$ (Fig. 6), the ionized gas has cooled adiabatically, with the overdense regions cooling at a slower rate than the underdense regions, as the more dense regions are better able to maintain thermal balance because of the shorter cooling (and photoionization heating) times. The IGM temperatures computed by the two simulations are now beginning to converge at high density, but at low density there is still a significant difference between the results. A third set of data points is also evident, corresponding to the latest locally underdense region to be ionized.

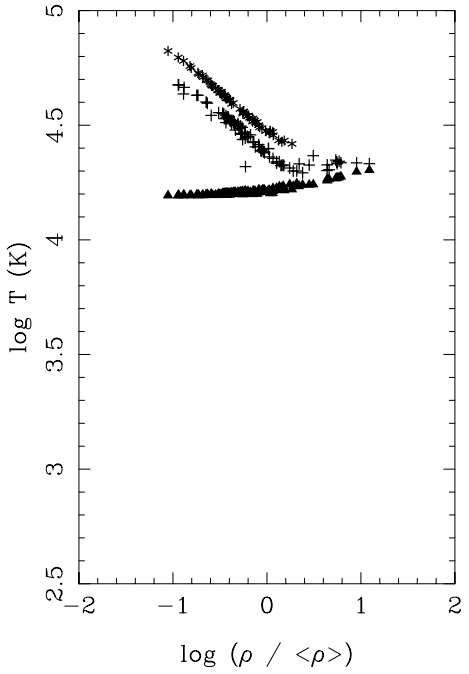

Figure 5. Comparison of the IGM temperature–density relation at $z = 5$ for regions with fully ionized helium ($n_{\rm He\,III}/n_{\rm He} > 0.9$). The triangles correspond to the uniform ionization case. The data points for the results incorporating radiative transfer are split into two sets:+ corresponds to gas in the range $10\,h^{-1} < R < 14\,h^{-1}$, for which the mean overdensity $\langle\rho/\bar{\rho}\rangle = 1.452$, (where $\bar{\rho}$ is the global mean gas density); and $*$ designates gas in the range $14\,h^{-1} < R < 23.6\,h^{-1}$, with mean overdensity 0.519.

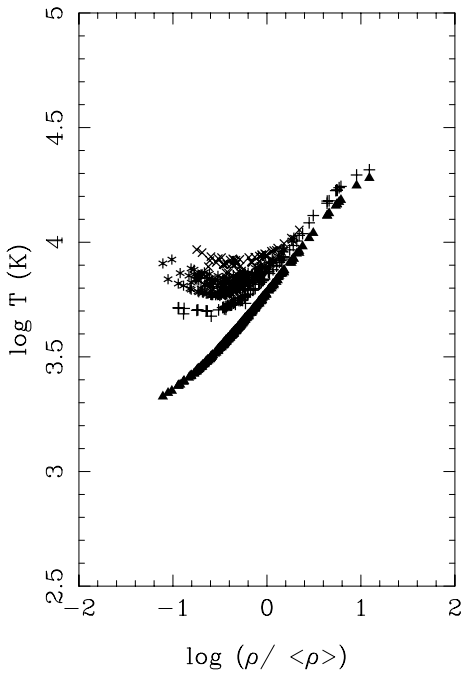

Figure 6. Comparison of the IGM temperature–density relation at $z = 3$. The symbols are as in Fig. 5. We also add a third point $\times$ designating gas in the range $23.6\,h^{-1} < R < 25.8\,h^{-1}$, with mean overdensity 0.671.

Finally, by $z = 1$, the gas temperatures computed by the RT and nRT simulations have nearly converged. The gradient of the line in the temperature–density plane indicates that adiabatic cooling caused by expansion is largely responsible for cooling the gas. We

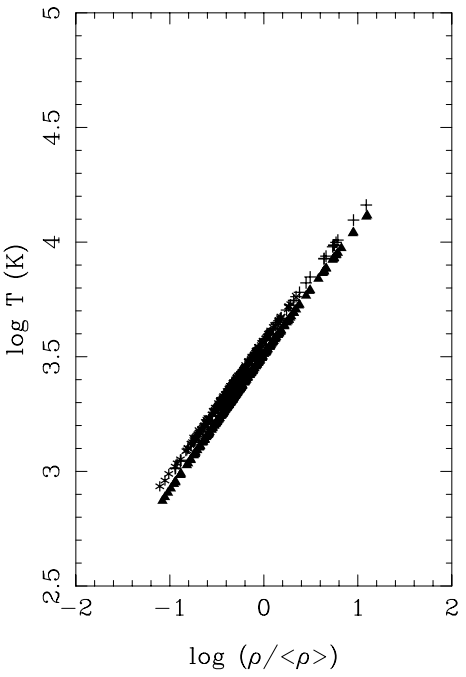

Figure 7. Comparison of the IGM temperature–density relation at $z = 1$. The symbols are as in Figs 5 and 6.

find that the entropy is now nearly constant throughout the line of sight. The striations in the RT data points have also disappeared. By $z = 1$, the results from the two simulations are in good agreement.

4 CONCLUSIONS

We extend the probabilistic method of radiative transfer described for hydrogen by Abel et al. (1999) to include helium and test the method on the propagation of an ionization front through a uniform medium. We compare the method against direct numerical integration of the exact time-steady radiative transfer equation. We confirm their conclusion that the probabilistic method accurately reproduces the position of the ionization fronts even for large optical depths at the photoelectric edges. Specifically, we recover the numerically integrated converged solutions for the ionization fractions and temperature to an accuracy of 10 per cent for an incremental optical depth per grid zone at the H I photoelectric edge as high as 20, while direct numerical integration of the radiative transfer equations requires an incremental optical depth of less than $1/4$ to obtain comparable accuracy.

We use the probabilistic method to compute the propagation of an I-front generated by a QSO source through the IGM, using the density distribution drawn from a numerical simulation in a ΛCDM universe. Including the effects of radiative transfer results in a substantial boost in the post-ionized gas temperature compared with the case of sudden uniform ionization with no radiative transfer. The boost chiefly results from the increased energy per photoionization within the ionization fronts, a consequence of the higher probability for high energy photons to pass through the gas compared with lower energy photons.

A consequence of the radiative transfer is to alter the dependence of temperature on density from the approximately polytropic relation found for moderate to low densities assuming uniform photoionization (Meiksin 1994; Gnedin & Hui 1998) to a generally non-monotonic trend. Although the differences between the temperatures for overdensities above ∼5 are small (less than 25 per cent), at lower densities the two temperatures converge only slowly with time, nearly recovering the polytropic relation only by $z \approx 1$.

At $z > 1$, the relation between temperature and density is not single-valued; multiple temperatures may result for different gas parcels of the same overdensity. Although this is in part a consequence of the delay in time for gas at different distances from the source to be photoionized as the ionization front propagates, an additional contributing factor is the environment of the gas parcel: if the ionization front has passed through a region of dense gas, sufficient to drive the optical depth at the H I photoelectric edge to near unity, before reaching the parcel, the radiation field will deliver a higher energy per photoionization to the parcel. Thus the determination of the gas temperature is strongly non-local because of the dependence of the heating rate on the optical depth to photoionizing photons between the gas parcel and the source of ionizing radiation.

Although the inclusion of radiative transfer results in a substantial and persistent boost in gas temperature, it is insufficient in itself to account for the broader measured Lyα absorption systems than predicted by numerical simulations assuming sudden uniform photoionization. Meiksin et al. (2001) find that a boost of $\Delta T \approx 1.7 \times 10^4$ K is required at $z \lesssim 3.5$, larger than the temperatures we find here. Although it may be possible to obtain a larger boost for an alternative reionization scenario, such a large boost may still require invoking late He II reionization. Our principal conclusion here is that for numerical simulations to predict the temperature of the IGM accurately, they must include the effects of radiative transfer. We are currently extending our methods to incorporate radiative transfer with ray tracing (e.g. Abel & Wandelt 2002) into fully self-consistent simulations to explore this and related issues, including alternative sources of reionization like low luminosity active galactic nuclei and stars.

ACKNOWLEDGMENT

A.M. thanks the University of Edinburgh Development Trust for its financial support.

REFERENCES

Abel T., Haehnelt M. G., 1999, ApJ, 520, L13
Abel T., Wandelt B. D., 2002, MNRAS, 330, L53
Abel T., Norman M. L., Madau P., 1999, ApJ, 523, 66
Anninos P., Zhang Y., Abel T., Norman M., 1997, New Astron., 2, 209
Bond J. R., Wadsley J. W., 1997, in Petitjean P., Charlot S., eds, Structure and Evolution of the Intergalactic Medium from QSO Absorption Line Systems. Editions Frontières, Paris, p. 143
Bryan G. L., Machacek M. E., 2000, ApJ, 534, 57
Cen R., Miralda-Escudé J., Ostriker J. P., Rauch M., 1994, ApJ, 437, L9
Ciardi B., Stoehr F., White S. D. M., 2003, MNRAS, 343, 1101
Croft R. A. C., Weinberg D. H., Katz N., Hernquist L., 1998, ApJ, 495, 44
Croft R. A. C., Weinberg D. H., Bolte M., Burles S., Hernquist L., Katz N., Kirkman D., Tytler D., 2002, ApJ, 581, 20
Gnedin N. Y., Abel T., 2001, New Astron., 6, 437
Gnedin N. Y., Hui L., 1998, MNRAS, 296, 44
Hernquist L., Katz N., Weinberg D., Miralda-Escudé J., 1996, ApJ, 457, L51
Madau P., Meiksin A., Rees M. J., 1997, ApJ, 475, 429
Meiksin A., 1994, ApJ, 431, 109
Meiksin A., White M., 2001, MNRAS, 324, 141
Meiksin A., White M., 2003, MNRAS, 342, 1205
Meiksin A., White M., 2004, MNRAS (astro-ph/0307289)
Meiksin A., Bryan G. L., Machacek M. E., 2001, MNRAS, 327, 296
Nakamoto T., Umemura M., Susa H., 2001, MNRAS, 321, 593

Peebles P. J. E, 1993, Principles of Physical Cosmology. Princeton Univ. Press, Princeton, NJ
Petitjean P., Mücket J. P., Kates R. E., 1995, A&A, 295, L9
Seljak U., McDonald P., Makarov A., 2003, MNRAS, 342, L79
Theuns T., Leonard A., Efstathiou G., 1998, MNRAS, 297, L49
Theuns T., Leonard A., Schaye J., Efstathiou G., 1999, MNRAS, 303, L58
Zaldarriaga M., Hui L., Tegmark M., 2001, ApJ, 557, 519
Zhang Y., Anninos P., Norman M. L., 1995, ApJ, 453, L57
Zhang Y., Anninos P., Norman M. L., Meiksin A., 1997, ApJ, 485, 496
Zhang Y., Meiksin A., Anninos P., Norman M. L., 1998, ApJ, 495, 63

This paper has been typeset from a TEX/LATEX file prepared by the author.